공학석사학위논문

Effects of Casing Roughness on Aerodynamic Performance in a Turbine Cascade

터빈 캐스케이드에서 케이싱의 표면 거칠기가 공력 성능에 미치는 영향

2014 년 8 월

서울대학교 대학원

기계항공공학부

안 영 모

Abstract

Effects of Casing Roughness on Aerodynamic Performance in a Turbine Cascade

Young Mo An

School of Mechanical and Aerospace Engineering

The Graduate School

Seoul National University

To investigate effects of casing roughness on aerodynamic performance especially secondary loss, four cases of experiment conducted in a linear turbine cascade. Smooth endwall case was the baseline. The others were roughness cases of 0.001, 0.002 and 0.005 of k_s/C size of roughness (sand grain) adhered to the endwall. One-dimensional hot wire anemometry of constant temperature anemometry applied for measurement of incoming endwall boundary layer and turbulence intensity. Total pressure and flow angle measured by 5-hole probe at the 1.2 axial chord (Cx) length downstream. Incoming endwall boundary layer thickness was increased but thickening boundary layer effect was negligible

considering 200mm of blade span while momentum thickness grew significantly. Mass averaged loss coefficient at 1.2Cx downstream of blade leading edge was increased by 38% from smooth case to 0.005 of k_s/C size of rough case. This increment was mostly due to stronger secondary motions of passage vortex and shearing motions between it and counter vortex which induced by higher level of incoming normal vorticity inside of incoming boundary layer as bigger size of roughness adhered. Increased roughness size on the endwall made greater velocity deficit toward the endwall so that incoming normal vorticity was grown. This greater incoming normal vorticity was the main reason of stronger streamwise voriticity rather than turning angle at the downstream according to classical secondary flow theory because changes flow exit angle was negligible. But overall loss was not continuously increased but saturated due to adverse effect between strengthen of incoming vortex and less vortex stretching. This was confirmed saturated circulations both passage and counter vortex area. Comparing inlet and downstream loss for smooth and rough cases, net increase in loss across the blade row was increased which was not similar as reported by many researchers for thin and thick boundary layer previously. It meant additional loss was raised through blade row. Higher mixing loss due to greater turbulence intensity inside incoming boundary layer by roughened tip endwall was thought to be the reason of additional loss.

Keywords: Casing Roughness, Secondary Loss, Passage Vortex, Turbine Cascade, Mass-averaged Loss Coefficient, Streamwise Vorticity

Student number: 2012-23174

Contents

List of Tables

List of Figures

Nomenclature

A	Area, m^2
C	Chord length, m
C_x	Axial chord length, m
C_p	Static pressure coefficient
$C\omega_s$	Streamwise vorticity coefficient
C_{SKE}	Secondary kinetic energy coefficient
H	Passage height, m
k_s	Equivalent sandgrain roughness, μm
P_s	Static pressure, Pa
P_t	Total pressure, Pa
Ra	Centerline averaged roughness, μm
rms	Root mean squre
S	Blade pitch, m
Tu	Turbulence intensity, %
U	axial velocity, m/s
x	Axial location from the leading edge, m
y	Pitch-wise location, m
Y_p	Total pressure loss coefficient
$\mathbf{z}$	Spanwise location from the hub endwall, m
β	Blade metal angle, ° (degree)
Γ	Circulation
δ	Boundary layer thickness, $y_{u=0.99U\infty}$
δ^*	Displacement thickness
θ	Momentum thickness
λ	stagger angle, ° (degree)
ρ	Fluid density
v	Fluid kinematic viscosity
ω_n	Normal vorticity
ω_s	Streamwise vorticity

Superscript

$\bar{}$	Mass averaged value

Subscript

1	Cascade inlet condition
2	Cascade outlet condition
MS	Mid span
SEC	Secondary velocity component at downstream measurement plane

1. Introduction

1.1. Background and motivation

The degradation of gas turbines both land based (normally for power generation) and propulsion with service is the serious problem in the efficiency point of view. This is mainly due to roughness on machine inside surface inevitably with operation. Therefore, study regarding surface roughness is important as well as machine's basic aerodynamic study at design stage. Such trend can be observed as increased number of paper issued at the journal [1]. Foreign particulates, air borne dusts, sand and even volcanic ash is the example of sources for surface roughness. Particularly in turbine side, because of the location, downstream of combustor, molten airborne contaminants agglomerate and adhere to turbine blade and casing. Thermal barrier coating (TBC) removal by spallation and hot corrosion are also the sources for roughening surface in turbine side. Fig. 1 shows a photograph of roughened turbine vane and endwall for serviced CFM56 engine [2].

This surface roughness changes boundary layer characteristics of both blade and endwall. Severely it can modify geometric parameters e.g. blade shape and incidence angle so that aerodynamic performances is dropped due to off-design conditions. Regarding aerodynamic performance, according to Denton [3], the overall loss consists broadly of profile loss, endwall loss and tip leakage loss. Profile loss is generated due to boundary layers on the blade surface away from the

endwall. Endwall loss is referred to as “secondary” loss because it arises from the secondary flows generated by endwall boundary layers and flow turning through blade rows. Tip leakage loss happens from the leakage flow over the tip through tip clearance between rotor and casing or stator and hub. Although these three loss components are described separately, it is hard to tell dividing those individually because those are having interaction each other. But overall loss is generally consisted of these three loss components evenly. Sjolander [4] schematically illustrates the mechanisms of loss generation in Fig.2.

Based on above performance degradation, surface roughness effects in gas turbine have been studied by many researchers but most of them are focusing on roughness on blade surface itself despite roughness elements are naturally on the endwall. Roughness on endwall also affects to change boundary layer developed by endwall and it would be strong influence to secondary loss.

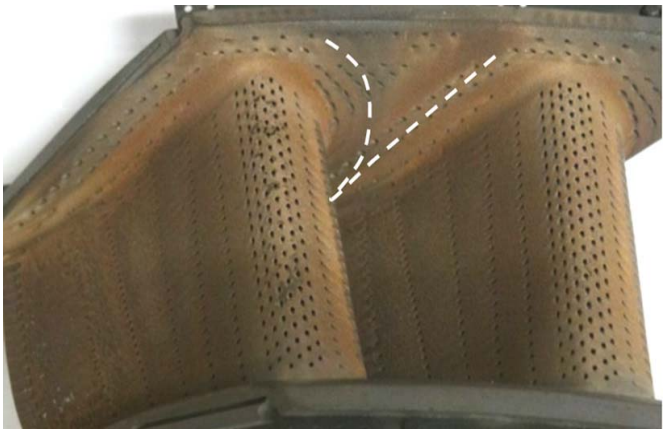

Fig. 1 Photograph of deposition on a serviced CFM56 engine’s turbine vanes [1]

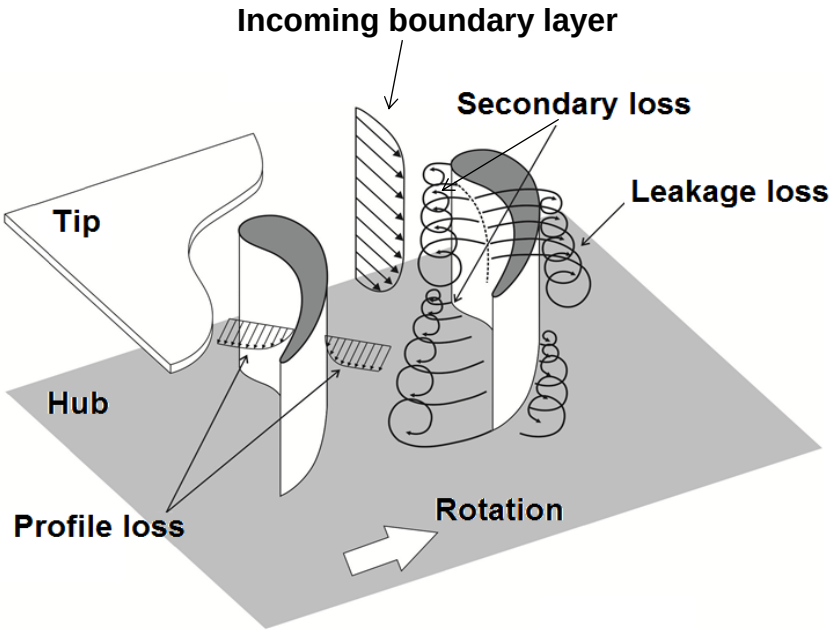

Fig. 2 Major loss components in turbomachinery by Sjolander [4] (Reproduced)

1.2. Literature Survey

Previous researches have been reviewed by two categories of surface roughness effects and aerodynamic loss, especially secondary loss.

Firstly, Surface roughness effects in gas turbine have been studied by many researchers. Prior to see effects of surface roughness, Bons et al. [5] provided accurate depiction of real surface roughness by measurements of nearly 100 in-serviced turbine components of four manufacturers: General Electric, Solar Turbines, Siemens-Westinghous and Honeywell. They suggested 26 representative statistical data grouped by roughness-generation process. But there was only single data group of endwall region by hot corrosion and erosion. Due to lack of information, this surface roughness data applied to in this study. Detail application can be referred to paragraph 2.4 below. Bones [1] also summarized the effects of surface roughness in gas turbine from other researchers. Most of studies for surface roughness effects are focused on roughness on blade itself despite it is on the endwall as well.

Rao et al. [6] have explored the influence of casing roughness in an axial flow turbine. They experimented with sandpaper to the casing with double-sided adhesive tape at different tip clearances. They obtained artificially roughening the casing surface significantly reduced the leakage mass flow rate and then this led deficit of momentum in the core of the tip vortex. This influenced tip vortex had

shearing interaction with passage vortex so that it cannot be distinguishable sole effect of casing roughness to passage vortex.

Matsuda et al. [7] measured the profile and secondary loss in a large scale vane cascade with varying degrees of surface polish of nozzle. They also compared total pressure loss between smooth and rough endwall. They found peak value of loss showed additional 30% of loss and moved it toward midspan. But they could not catch secondary flow structures but just recognizable those by total pressure loss contours due to relatively low flow turning angle. They neither explained how the roughened endwall affect the formation of secondary flow structure and why this additional loss was happened.

Regarding secondary flow and loss, there have been a lot of researches up to now. Squire and Winter [8] were the front runner of secondary flow research. They proposed simple estimation for streamwise vorticity generation under inviscid and incompressible flow which has been widely used for estimation of streamwise vorticity generation. Hawthorne [9], [10] later developed a general theory for secondary flow of an inviscid, incompressible fluid and three components of vorticity. The first was distributed secondary circulation which was the result of a distortion of the vortex filaments carried with the stream through bending passage. This appeared as passage vortex at the exit of the cascade. The second component was the trailing shed circulation due to the change of circulation about body

immersed in the flow. Finally the third component was the trailing filament circulation which arose because stretching of the inlet vortex filament when passing through the cascade. A method had been described for calculating the secondary flow in a cascade, taking into account the rotation of Bernoulli surface [11]. This study showed a good estimate of the secondary flow was obtained if distortion of the Bernoulli surface was neglected.

Detail secondary flows and losses in a turbine cascade had been found by experiments of flow visualizations by use of oil and smoke or total pressure measurement traversing at several planes in axial direction within a cascade passage in the early stage of secondary flow research. Flow visualization had been done both endwall surface and blade pressure and suction surface. Langston et al. [12] and Marchal and Sieverding [13] and Gregory-Smith and Grave [14] gave good interpretation and enhanced understanding of developing secondary flow through a turbine cascade. Sieverding [15] had summarized the results of previous experimental works for secondary flow. It presented secondary vortex structures and their effect on endwall boundary layer characteristic and loss growth through a turbine cascade. After 15 years past, Langston [16] had also issued review paper for building upon Sieverding's review and to examine some of the secondary flow research since its publication. Hodson and Dominy [17] gave wide insight of

cascade performance, not even secondary flows, by conducted experiments at various off-design conditions.

Lastly, Hunter [18] had conducted experiment in an axial turbine stage of two different incoming endwall boundary layer thicknesses. The amounts of over and under-turning in the stator exit flow were decreased due to reduction in te inlet normal vorticity associated with the thicker and more rounded velocity profiles of thicker boundary layer thickness of incoming flow. Pichwise averaged total pressure loss data indicated that the net cascade passage losses are independent of the cascade inlet boundary layer thickness. Sharma and Butler [19] had reported same result as above from summarized those of other researchers [12], [13], [14], [17].

1.3. Objectives

Despite many researches for surface roughness and secondary flow in a turbine cascade, the effects of casing roughness on aerodynamic performance in a turbine cascade are not examined. Therefore, the present study aims to investigate effects of casing roughness by sand grain on the cascade endwall on aerodynamic performance, especially secondary loss in a linear turbine cascade with no tip clearance. For achieving above, aerodynamic performance e.g., secondary loss and flow turning angle is evaluated by measuring total pressure distribution at the downstream of a turbine rotor blade row in a linear cascade. Smooth casing is the baseline while three different size of sand grain is adhered to the cascade tip endwall as casing roughness.

Therefore research objectives for this study are following:

1. The effects of casing roughness on secondary loss change.
2. The effects of casing roughness on incoming endwall boundary layer characteristics.
3. The relation between change in secondary loss and incoming boundary layer induced by casing roughness.

2. Test Facility and Instrumentation

2.1. Test Facility

Fig. 3 schematically shows a test facility, consisting of (a) an AC motor and centrifugal fan, (b) a diffuser, (c) a settling chamber, (d) a contraction section, (e) a flow developing section, and (f) a test section. Centrifugal type fan with 15kW electric motor can produce up to 300 m3/min. of volume flow rate. The fan blows into settling chamber containing four mesh screens and honey comb through diffuser and the flow exits the contraction through a 200 x 500mm outlet section. Flow developing section is changeable according to test section and connects wind tunnel and test section. Wind tunnel is designed to produce flow of maximum velocity 55m/s with turbulence intensity 0.6%. The linear turbine cascade type with 8 blades and 7 passages is installed on the open type wind tunnel of described above.

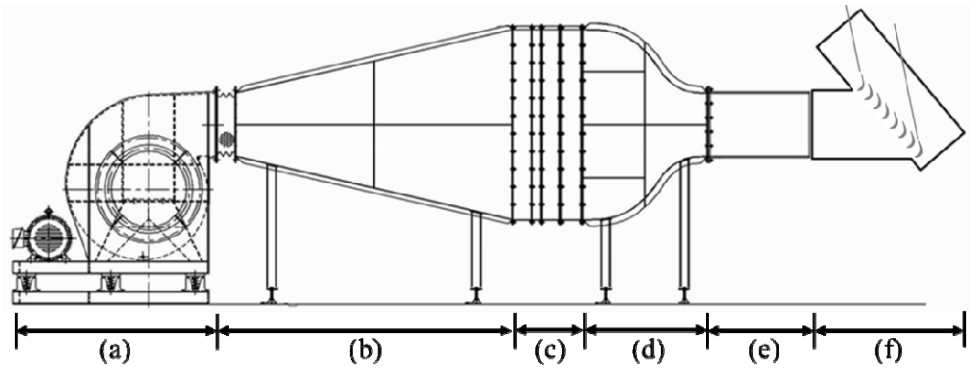

Fig. 3 Schematic of test facility showing a test section accommodating a linear cascade

2.2. Blade Geometry

Blade geometry is referred to Large Scale Rotating Rig at United Technologies Research Center [20]. The rotor blade mid-span profile is used to build this linear turbine cascade. Details of blade are shown in Fig. 4 and Table 1.

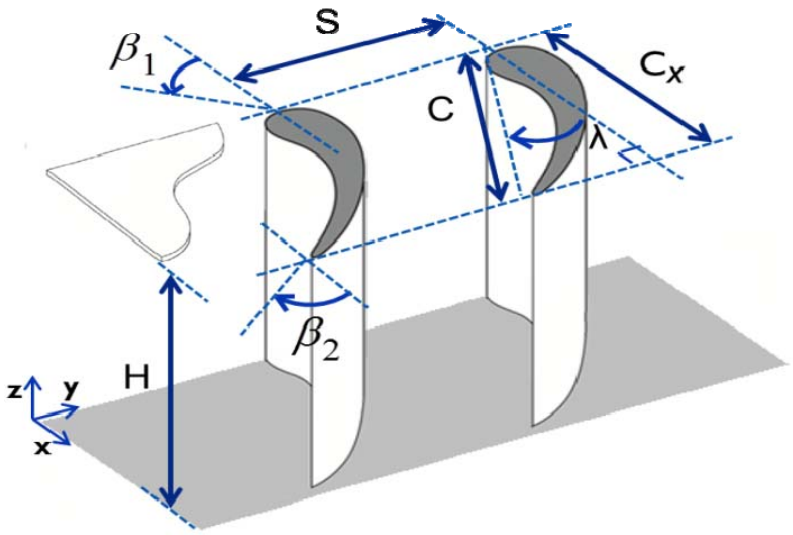

Fig. 4 Schematic of the blade geometry

Table 1 Geometric parameters of the blades

Chord length, C	109.58 mm
Axial Chord length, C_x	93.41 mm
Stagger angle, λ	32.12º
Span, H	200 mm
Pitch, S	92.34 mm
Solidity, C/S	1.19
Inlet flow angle, β_1	42.18º
Outlet flow angle, β_2	-64.03º

2.3. Instrumentation and Data Acquisition

The schematics of cascade and measuring points are shown in Fig. 5. Inlet total and static pressure was measured using Pitot probe (United Sensor™) at $0.7\,C_x$ upstream from the blade leading edge which is point no.1 of Fig. 5. Inlet endwall boundary layer and turbulence intensity was traversed using one dimensional hot wire probe of 55P11 type (Dantec Dynamics™) at point no.2 of Fig. 5 which is at mid-passage of blade leading edge line between 5th blade and 6th blade. Hot wire probe was connected to constant temperature anemometry system. Measurements were made by collecting 50,000 samples at a rate of 10kHz at each points where approaching to tip endwall. The calibration of the 55P11 type hot wire probe was done both before and after measurements by auto calibration kit. Auto calibration kit could produce air of controlled velocity through nozzle if compressed air was supplied properly. The velocity calibration range was from 0 to 40 m/s. Calibration curve was obtained by 5th polynomial curve pitting at every experimental cases. The conservative estimated uncertainties of the measured velocities and turbulence intensities were ±0.2 m/s and ±0.3%p with a 95% confidence interval, using the method of Coleman and Steele [21], respectively.

At $1.1\,C_x$ downstream from blade leading edge, point no.4 of Fig. 5, periodicity was confirmed through hub endwall static pressure taps along the three passages from 3th blade to 6th blade. Periodicity was controlled by adjusting each

tail boards. The peak value difference of static pressure coefficients C_p was 2.4% which was enough to precede main experiment.

Downstream total pressure loss and flow angle was measured by conical shaped five hole pneumatic probe (United Sensor™) at $1.2\,C_x$ downstream from blade leading edge. The calibration and data reduction procedures for five hole probe was adapted from Judd. A. M. [22], Everett et al. [23] and Kim and Kang [24]. The estimated uncertainties [21] associated with loss coefficient and flow angles were evaluated to be within ± 0.002 and ± 1.0 degree, respectively.

Downstream measurement plane was made by two axis automatic traversing system controlled by program of National Instruments Corp. LabVIEW™. This measurement plane consisted of both 34 points along the pitchwise and 28 points of half span and total 952 points. It was described at Fig. 6. To obtain detailed flow features changes, measuring grid were set denser both at tip and blade trailing edge region. Spatial resolutions at denser region were $\Delta y/s = 0.027$ and $\Delta z/H = 0.0165$.

Casing roughness was realized by adhering sand grain on the tip endwall by one chord length long from 5mm of blade leading edge upstream after spraying glue on it. Aparting 5mm from blade leading edge line was for hot wire measurement. Using sand grain was the way of avoiding step effect when sand paper applied on the tip endwall. Casing roughness covering length was set to one

chord length long by assuming actual distance from combustor exit to turbine first rotor blade. Casing roughness was described at Fig. 5 (a).

Pressure Systems Inc. Net Scanner™, as differential pressure transducer was used for both pneumatic probes and static pressure taps. The specification of the sensor range was ±2.5kPa and uncertainty was ±0.5% of full scale.

For all cases, upstream velocity was set as 30 m/s and Reynolds number based on chord length and upstream velocity was 220,000 which was over the range where almost constant total pressure loss was marked when Reynolds number increase [25].

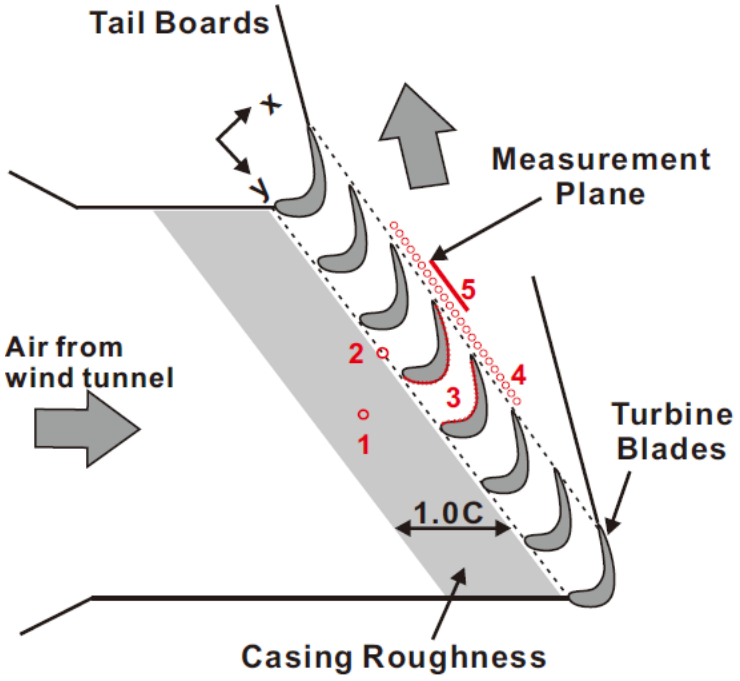

(a)

(b)

Fig. 5 Schematics of turbine cascade; (a) measuring points and roughness location, and (b) picture of sand grain adhered on the tip endwall view from upstream side

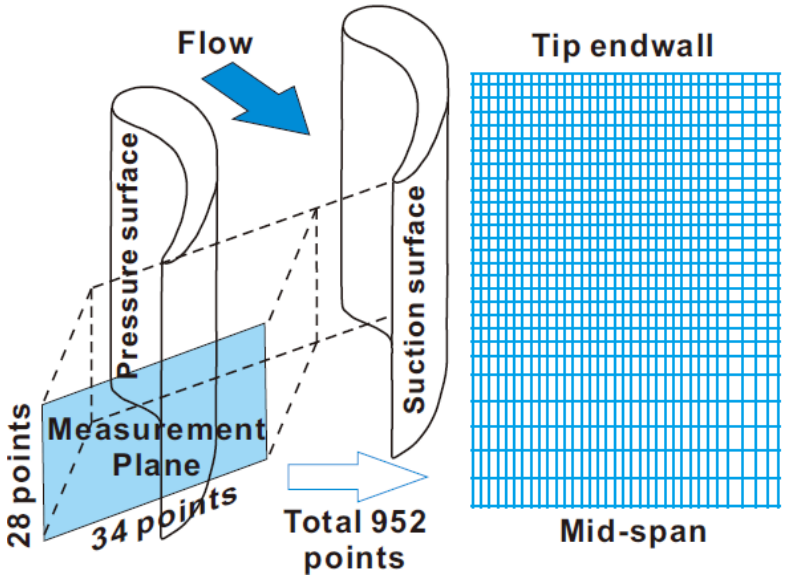

(b)

Fig. 6 Schematics of turbine cascade; (a) measuring points and roughness location, and (b) downstream measurement plane

Table 2 Instrumentations

No.	Measured	Instrument	Location
1	Inlet Pt & Ps	Pitot tube	0.7Cx upstream
2	Boundary layer	Hot wire	Mid-passage
3	Blade loading	Static taps	Midspan of blade pressure and suction surface
4	Periodicity	Static taps	1.1Cx downstream
5	Downstream loss	5-hole probe	1.2Cx downstream

2.4 Test Matrix

Table 3 is showing test matrix of different size of roughness cases. Roughness size is selected based on one of measurements of surface roughness of in-serviced gas turbine by Bons et al. [5]. “Surface #15” among 26 representative three-dimensional surface statistical data grouped by roughness-generating process, which is describing regarding endwall indicates 28 ㎛ of centerline average roughness (*Ra*). Equivalent sandgrain roughness (k_s) is obtained 173.6 ㎛ by Koch and Smith correlation [26]. This corresponds with test matrix no. 3 of 180 ㎛ of k_s, on Table 2. Because there are largely absent near suction surface on the endwall scrubbed by horseshoe and passage vortices [27], larger and smaller size of roughness element is required to check roughness effect more clearly, which are 500 ㎛ of k_s, no. 4 and 105 ㎛ of k_s, no. 2 of test matrix on Table 3. Smaller size of roughness (k_s =105 ㎛) on the other hand, takes from the observation of Bammert and Sandstede [28]. They suggest maintaining turbine surface below k_s / C of 0.001 in order to avoid efficiency drop. Although they artificially roughened turbine blade surface, it is inevitable to select as minimum size of roughness to see the endwall roughness effect due to lack of endwall roughness measurements.

Table 3 Test Matrix

No.	Case	k_s (μm)	k_s / C
1	Smooth	No sand grain adhered	0
2	Rough 1	105	0.001
3	Rough 2	180	0.002
4	Rough 3	500	0.005

2.5. Data Reduction Parameters

2.5.1 Turbulence intensity (Tu)

The nature of the turbulence in a wind tunnel of conventional design can be expected to be homogeneous and nearly isotropic states [29]. Tu is defined as Equation 1.

$$\mathrm{Tu} = \frac{\sqrt{u_{rms}^2}}{V} \tag{1}$$

2.5.2 Loss coefficient (Y_p)

Loss coefficient (Yp) is defined as Equation 2. Difference between $0.7\,C_x$ upstream and $1.2\,C_x$ downstream total pressure is non-dimensionalized based on mixed out velocity dynamic head.

$$Y_P = \frac{P_{t1,MS} - P_{t2}}{\frac{1}{2}\rho V_{mixedout}^2} \tag{2}$$

2.5.3 Mass-averaged loss coefficient (Y_p)

Overall loss level can be evaluated using mass-averaged loss coefficient. Mass averaged loss coefficient is defined as Equation 3.

$$\overline{Y_P} = \frac{P_{t1,MS} - \overline{P_{t2}}}{\frac{1}{2}\rho V_{mixedout}^2} \tag{3}$$

2.5.4 Secondary kinetic energy coefficient (C_{SKE})

The secondary kinetic energy coefficient represents the kinetic energy associated with secondary velocity vectors, not the primary direction normalized by the kinetic energy on the inlet midspan of the cascade. The increment or reduction can attribute to secondary loss increase or decrease. This is defined as Equation 4 below.

$$C_{SKE} = \frac{{v_{sec}}^2 + {w_{sec}}^2}{{V_1}^2} \tag{4}$$

2.5.5 Circulation (Γ)

The circulation which is normalized by axial chord length and cascade inlet velocity represents the strength of vortex. This parameter can be used as comparing the strength of vortices measured at downstream measurement plane quantitatively. This is defined as Equation 5 below.

$$\frac{\Gamma}{C_x V_1} = \frac{1}{C_x V_1} \iint_A \omega_x \bullet dA \tag{5}$$

2.5.6 Derivation of Streamwise Vorticity

Streamwise vorticity coefficient is calculated according to the method of Gregory-Smith et al. [30]. This is derived from the incompressible Euler equations and it is useful for identifying vertical structures and quantifying their strength and

sense of rotation. This method is verified of measuring at two closely spaced axial planes by Yaras and Sjolander [31]. They reported largest differences between actual measurements and approximation by this method was comparable with the uncertainty. This method has been widely selected by many researches. This is defined as Equation 6 below. Fig.7 shows exit flow coordinate system for streamwise vorticity coefficient calculation.

$$C\omega_s = C\omega_x \cos\overline{\beta_2} + C\omega_y \sin\overline{\beta_2}, \quad (C\omega_x = \frac{\omega_x C_x}{V_{inlet}}, \quad C\omega_y = \frac{\omega_y C_x}{V_{inlet}}, \quad \overline{\beta_2}: \text{mass averaged flow exit angle}) \tag{6}$$

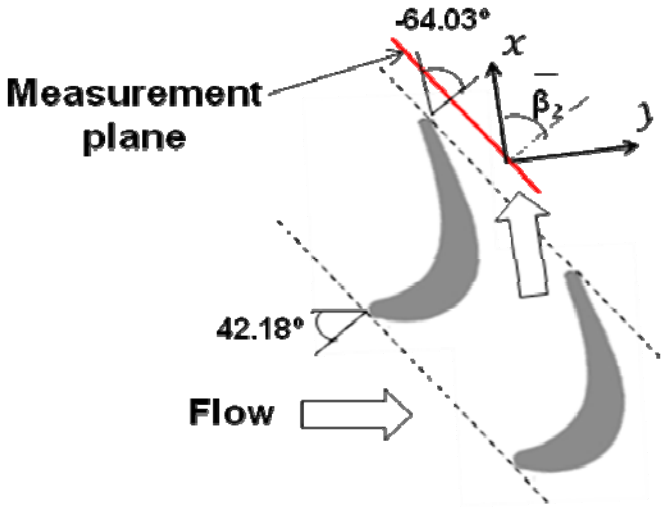

Fig. 7 Flow coordinate systems at cascade exit for streamwise vorticity coefficient calculation

3. Discussion of Results

3.1. Mass averaged loss coefficient

To investigate how casing roughness affect to overall aerodynamic loss at downstream, mass averaged loss coefficients at 1.2Cx downstream from leading edge are reported for each case. Fig. 8 shows increasing mass averaged loss coefficients as bigger roughness size adhered to the endwall. Mass averaged loss coefficient of 0.043 for smooth case is almost same as previous turbine cascade studies [32], [33]. 27% of loss increment occurs from smooth to rough 2, from 0.043 to 0.054. In order to figure out what causes this loss increment, total pressure loss contours examined.

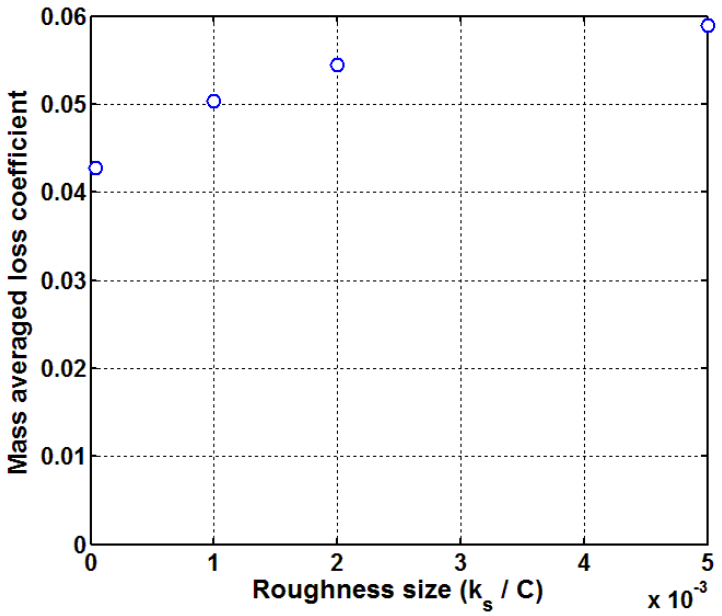

Fig. 8 Mass averaged loss coefficients according to different roughness size

3.2. Loss coefficient contours

Loss coefficient contours with flood are easy to catch spatial variation between smooth to rough case. Total pressure loss coefficient contour with flood at 1.2Cx downstream of blade leading edge is provided in Fig. 9. The view is looking upstream with passage suction surface on the left and pressure surface on the right. White region of Fig. 9 is no loss region. There are two distinct regions of elevated loss labeled A and B in Fig. 9 (a). Loss core A located at the y/S=0.13 and z/H=0.87 is associated with the passage vortex which is combination of low momentum fluid from endwall boundary layer and pressure side leg of horse shoe vortex from the adjacent blade leading edge. Another peak loss core B is the one by shearing motion between passage vortex and trailing vortices (trailing filament and trailing shed vortex). These trailing vortices could not be caught by secondary velocity vectors of red arrows as full vortex motion at Fig. 11 but assuming it by location within wake region according to secondary flow theory. These trailing vortices are sometimes so weak that those could not be caught by secondary velocity vector as a complete vortex motion. In this case, these are called just counter vortex [34]. These loss cores can be categorized to secondary loss. Loss core A is occupied wider and peak loss is greater at rough 2 case than smooth case. Wider occupying area of passage vortex can be considered as effect of thicker incoming boundary layer [17] but increased peak strength of passage vortex cannot

be explained by it. So this is different from the effect of thicken incoming endwall boundary layer effects, i.e. wide occupying area by passage vortex but weaken peak strength of vortex, same effect of vortex stretching. Peak loss of loss core B is also greater than smooth case but occupying area cannot be told because of location, inside of wake region. But the location of peak loss area moves toward midspan when smooth to rough 2 case. This is due to greater penetration height toward midspan of passage vortex and suction side of horse shoe vortex separation line by thicken incoming endwall boundary layer [19]. Also another loss core beneath loss core B is visible. This loss core is appeared to develop so it becomes isolated from smooth to rough 2 case. This is due to stronger suction side leg of horse shoe vortex likewise stronger passage vortex of rough 2 case because both pressure and suction leg of horse shoe vortex is from mostly incoming boundary layer fluid. This is also different phenomena from effect of higher Reynolds no. to prevent separation of the suction surface boundary layer [17]. In rough case 2, streamwise velocity at downstream measurement plane is not greater than that of smooth case.

In order to figure out secondary loss separately, profile loss measured at midspan has to be deducted from the total measured loss. Measured profile loss is expressed as mass averaged loss coefficient at midspan.

$\overline{Y_{P,MS}} = 0.025$ for smooth, $\overline{Y_{P,MS}} = 0.031$ for rough 2

Profile losses measured at midspan remains over the range of measuring uncertainty. Profile loss is increased as it goes from smooth to rough 2 case. It can be confirmed by thickened wake width at midspan on loss coefficient contour on Fig. 9 (b). This profile loss increments was also found previous literatures [12], [35]. This is because the boundary layers which developed both suction and pressure surface in the midspan regions are influenced by the endwall secondary flow effects of incoming endwall boundary layer. To find out in details the reason why profile loss is increased is to do more experiments for measurement of blade boundary layers by flow visualization using oil or others for looking into profile loss increase. But this is beyond the aims of this study of focusing on secondary loss. Pitchwise averaged mass averaged loss coefficients distribution along with the spanwise location is presented secondary loss only as Fig. 10, which is deducted from overall loss to profile loss. Loss coefficients of area from z/H=0.7 to 0.9 associated both loss core A and B at rough 2 case are higher than smooth case. Loss coefficients at rough 2 case from z/H=0.83 to 0.9, loss core A associated with the passage vortex marks higher than smooth case and those from 0.75 to 0.83, loss core B also indicates greater than smooth case. These higher losses are also confirmed secondary kinetic energy coefficient contours of Fig. 11 (a) and (b).

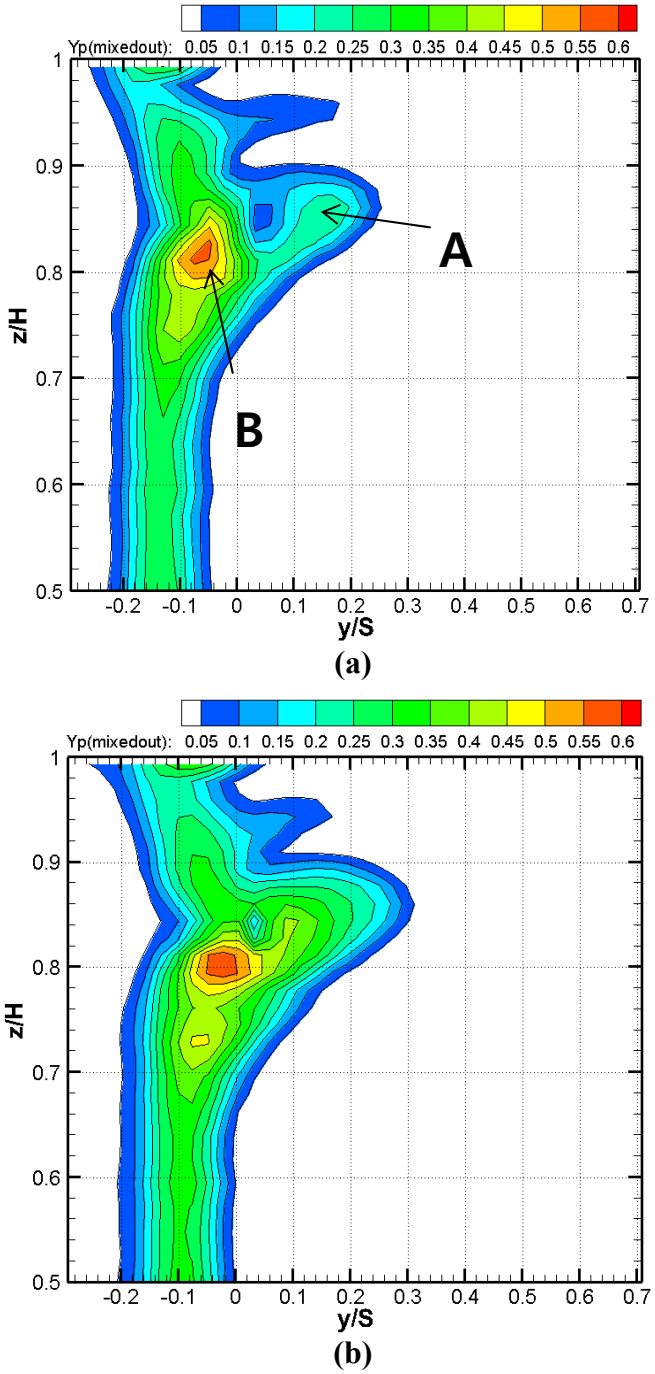

Fig. 9 Loss coefficient contours with flood at 1.2Cx downstream of blade leading edge; (a) smooth (baseline) and (b) rough 2

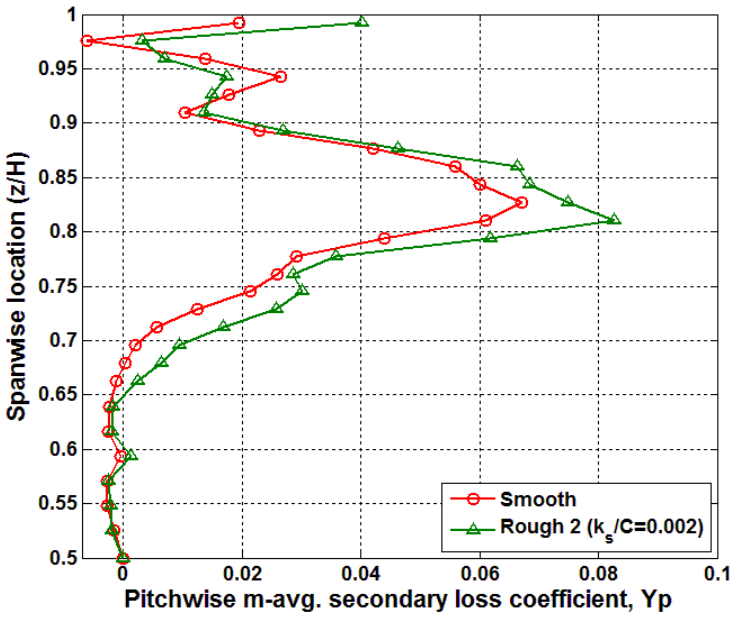

Fig. 10 Pitchwise mass averaged loss (secondary loss only) coefficients distribution of smooth and rough 2 case along with spanwise location at 1.2Cx downstream of blade leading edge

Red arrow is indicating secondary velocity vectors with 10m/s magnitude of reference vector at the right top corner. By stronger secondary velocity vectors and higher C_{SKE} near endwall (from z/H=0.94 to 0.99), Higher cross flow velocity from pressure to suction surface is shown at rough 2 case rather than smooth case. Stronger passage vortex motion leads this bigger velocity of cross flow. This stronger passage vortex motion also collects more low momentum fluid from the endwall boundary layer so that higher shearing motion between passage vortex and trailing vortices is marked at loss core B. Higher secondary velocity vectors also confirm this stronger shearing motion.

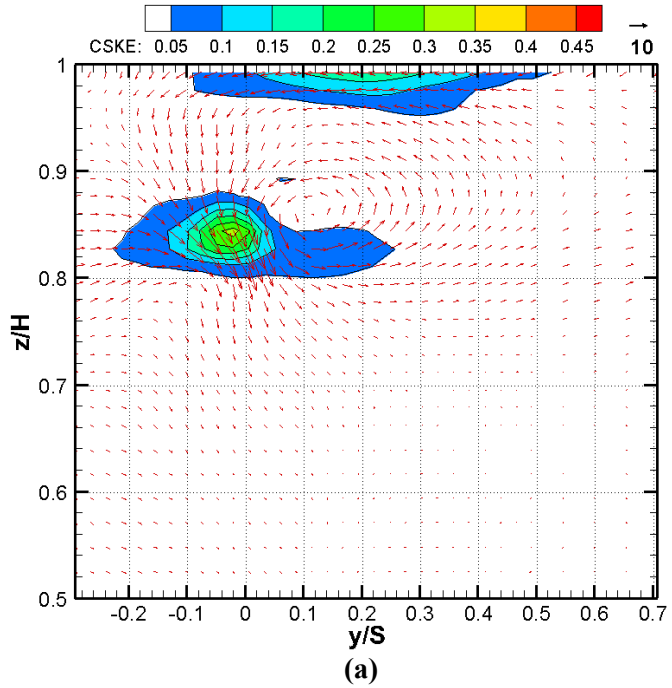

Fig. 11 Secondary kinetic energy coefficient contours with flood at 1.2Cx downstream of blade leading edge; (a) smooth (baseline) and (b) rough 2

3.3 Streamwise vorticity contours and circulations

By employing surface roughness at the cascade tip endwall, mass averaged loss coefficient at 1.2Cx downstream from blade leading edge is increased and this increment is confirmed by stronger passage vortex and shearing motion between passage vortex and trailing vortices as above. To analyze these loss cores quantitatively, streamwise vorticity coefficient contours and circulations for each loss core are represent as Fig. 12 and Fig. 13. Loss core A and B of rough 2 case shows higher streamwise vorticity levels than those of smooth case at Fig. 12. These higher streamwise vorticity indicate stronger secondary motions which are identified by bigger secondary velocity vectors of red arrow on Fig. 12 (b). Stronger secondary motions make higher shear around secondary flow structures so that loss, in this case secondary loss increases. This rise of secondary loss is the major for growth of mass average loss coefficients at measurement plan of 1.2Cx downstream from blade leading edge.

Another way of checking increased secondary loss is comparing circulations of each loss core. Circulation is the quantitative values of vortex strength. In this study, circulation normalized by incoming velocity and axial chord length is applied. Fig. 13 shows normalized circulations of loss core A and B. Loss core A which associated with passage vortex shows positive circulation because it rotates counter clockwise at Fig. 13 and vice versa for loss core B.

Stronger passage vortex appears at rough 2 case than smooth case. Circulation for loss core B at rough 2 case is also stronger than smooth as well but absolute value of loss core A is bigger than loss core B. This means loss core A leads for increasing overall loss dominantly. Normalized circulation both loss core A and B is continuously raised but saturated as bigger roughness element adhered. This saturation of both loss cores' circulation can explain the reason why overall loss saturation at Fig. 8 above. The reason of saturation of circulations is thought to be combine effect of less vortex stretching and strengthen of vortex within inside of incoming endwall boundary layer. Even though strength of incoming vortex is greater by surface roughness which confirmed by Fig. 15 below, streamwise velocity of both loss core A and B at downstream measurement plane is reduced as it goes to bigger rough cases. This reduced velocity leads to less vortex stretching effect. Above adverse effect between strengthen of incoming vortex and it's less stretching makes circulation saturate, not continuously increase.

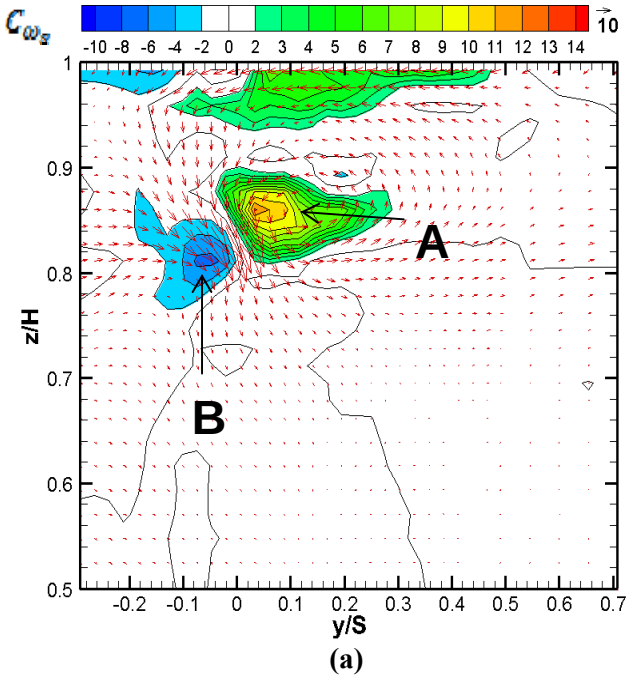

(a)

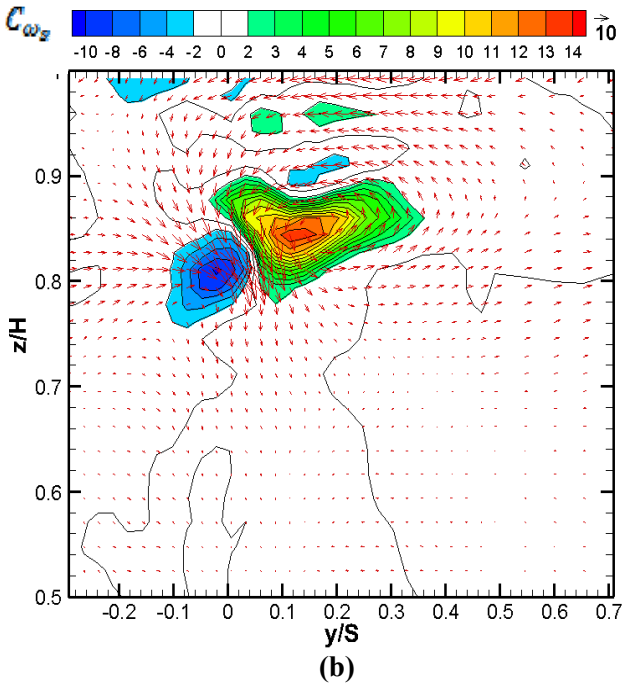

(b)

Fig. 12 Streamwise vorticity coefficient contours with flood at 1.2Cx downstream of blade leading edge; (a) smooth (baseline) and (b) rough 2

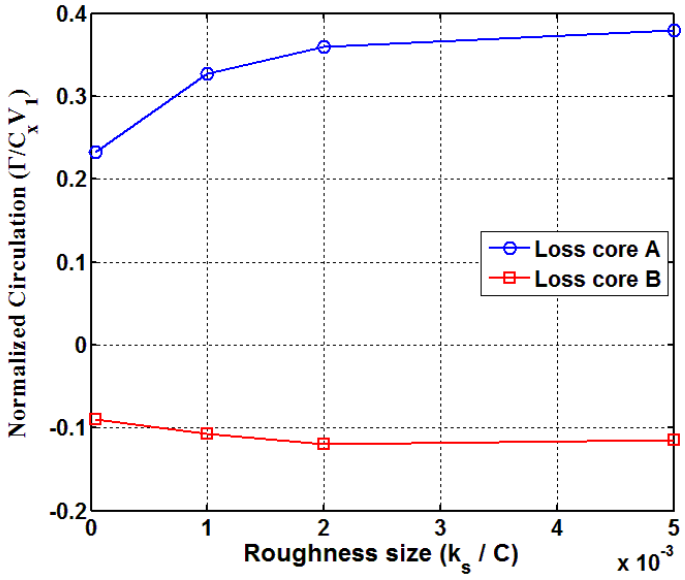

Fig. 13 Normailized circulations according to roughness size at 1.2Cx downstream of blade leading edge

3.4 Flow turning characteristics

As above, it is examined how overall loss is affected by casing roughness of employing sand grain on cascade endwall and secondary loss, especially loss associated with passage vortex is the major contribution for overall loss increase. The Squire and Winter approximation [8] is applied to find out the reason why this stronger passage vortex happened. Equation below, known as the Squire and Winter approximation is considered wide application in the estimation of streamwise vorticity generation.

$$\omega_s \approx -2\Delta\theta \cdot \omega_i,$$

$\Delta\theta$ is the bending angle which is considered as turning angle through cascade and ωi is the inlet vorticity which is inlet normal vorticity (ω_n) due to two dimensional incoming flow. According to study of them, streamwise voriticity is proportional to product of free stream turning angle and inlet normal vorticity. Both flow turning angle and inlet vorticity is the possible reasons of higher streamwise vorticity by rough 2 case at Fig. 12 (b) above.

Firstly, examining turning angle, pitchwise mass averaged flow exit angle at 1.2Cx downstream from blade leading edge represents at Fig. 14 (a). Free stream turning angle measured near midspan between smooth and rough 2 case remains within the measuring uncertainty. It means casing roughness by sand grain on endwall does not affect free stream turning angle, thus casing roughness does not

affect streamwise vorticity change at downstream in the point of free stream flow turning through cascade blade. The difference between under turning degree which associated with loss core A and B for smooth and rough 2 case is maximum 1.3°, which is negligible considering measuring uncertainty of ±1.0°. Fig. 14 (b) shows mass averaged deviation angles according to endwall roughness size from smooth to rough 1, 2, and 3. There is no significant difference between smooth and rough 2 case. Based on review of flow turning characteristics, it is known that $\Delta\theta$ is not the major parameter for higher streamwise vorticity at downstream measurement plane.

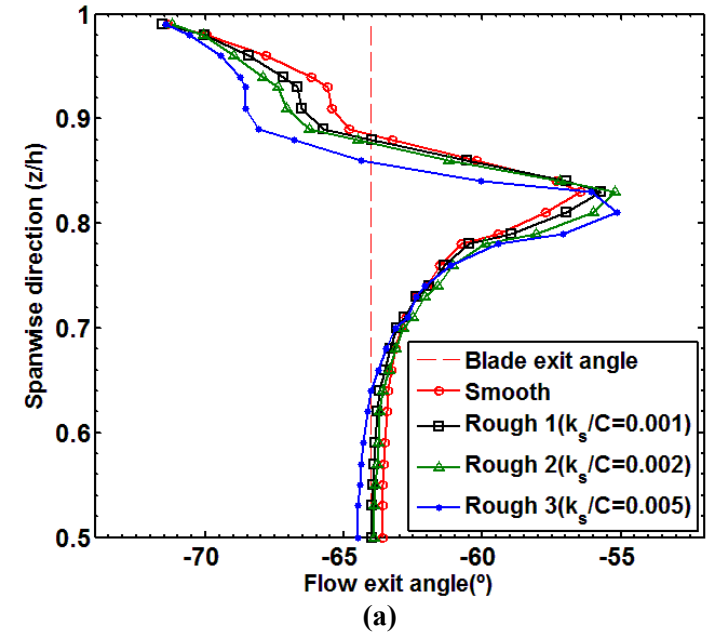

(a)

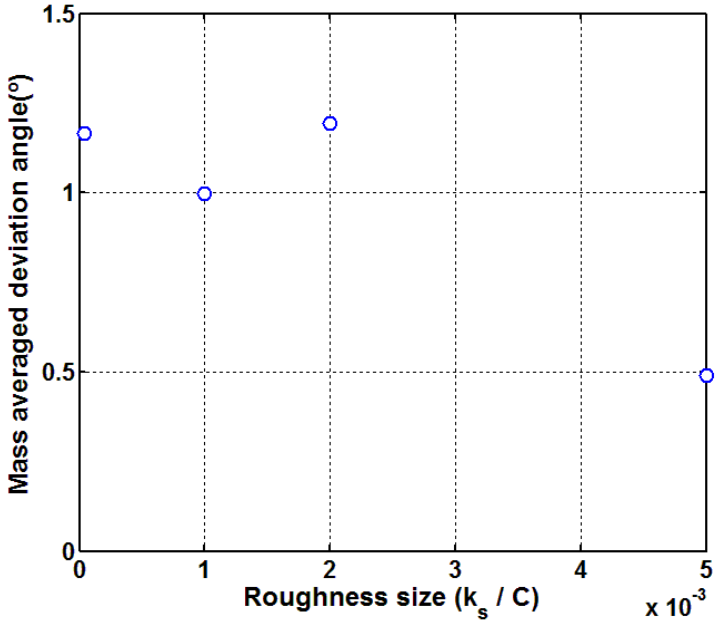

(b)

Fig. 14 Flow turning characteristics according to roughness size from smooth to rough 1, 2 and 3 at 1.2Cx downstream of blade leading edge; (a) Pitchwise average flow exit angle distribution along the span and (b) Mass averaged deviation angles

3.5 Incoming flow characteristics

To figure out the reason of higher streamwise vorticity of passage vortex, flow turning angle has been review according to Squire and Winter approximation above. Another parameter of their approximation is inlet normal vorticity (ω_n). Assuming incoming flow as two dimensional uniform flow, inlet vorticity has just normal vorticity component only within the endwall boundary layer. Inlet normal vorticity distributions within endwall boundary layer are shown on Fig. 15. Incoming normal vorticity of mean velocity for rough 2 case marks higher than smooth case. Eventually this higher incoming normal vorticity is the reason for higher streamwise vorticity at downstream measurement plane.

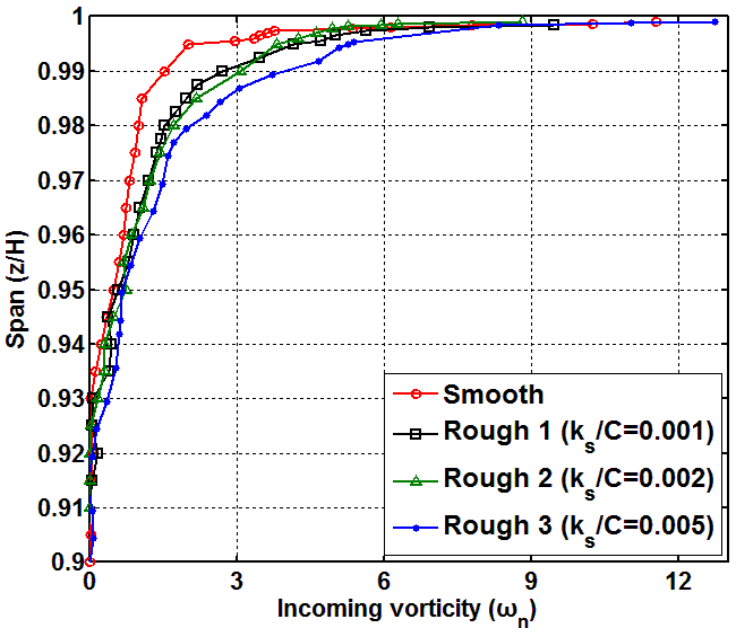

Fig. 15 Incoming normal vorticity distributions along with spanwise location at mid passage of leading edge line of blade

This higher incoming normal vorticity is caused by greater velocity deficit toward endwall inside of boundary layer. Incoming endwall boundary layer profiles are shown on Fig. 16. Velocity deficit at rough case 2 is greater than that of smooth case. Momentum loss due to surface roughness elements on endwall leads bigger velocity deficit. Growing momentum loss from smooth to rough 2 case could be confirmed by calculations of integral parameters of incoming endwall boundary layer at Table 4. Displacement and momentum thickness is getting thicker as roughness size on endwall is getting bigger. By shape factors at Table 4, all cases incoming flow are already turbulent based on shape factors. Boundary layer thickness also becomes thicker but it is hard to tell the differences by considering 200mm length of blade span. Therefore effects of variation of incoming endwall boundary layer thickness is not shown, which reported as wide area occupied by passage vortex but peak strength of it is reduced [17].

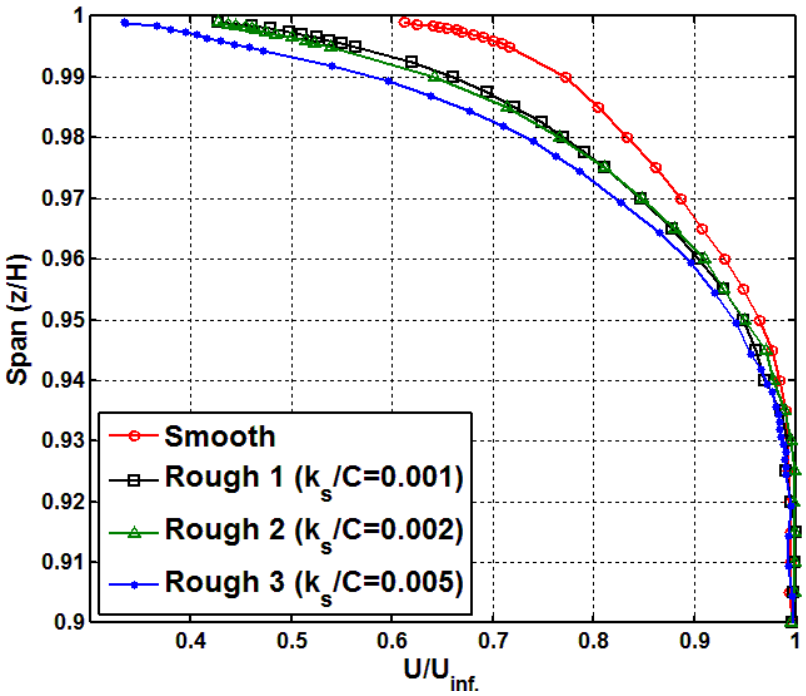

Fig. 16 Incoming endwall boundary layer profiles

Table 4 Integral parameters and shape factors of incoming endwall boundary layer

Case	Smooth	Rough 1	Rough 2	Rough 3
Boundary layer thickness (mm)	12.9	13.7	14.1	14.6
Displacement thickness (mm)	1.66	2.38	2.78	2.81
Momentum thickness (mm)	1.29	1.65	1.76	1.78
Shape factor	1.29	1.45	1.58	1.58
$2\delta / H$	0.129	0.137	0.141	0.146

3.6 Net Loss Increase Through Cascade

Fig. 17 shows mass averaged total pressure loss growth from 0.7Cx upstream to 1.2Cx downstream of blade leading edge. Fig. 17 (a) is reproduced the results of thin and thick incoming boundary layer from Gregory-Smith and Grave [14]. Loss increment between thin and thick boundary layer at inlet is almost same at downstream. Loss slope is not changed. This means inlet vorticity change by thin and thick boundary layer does not affect additional loss generating. But when roughness is on the casing wall, loss gap at inlet between smooth and rough is increased at downstream. Slope is getting steeper. It tells additional loss happened through cascade. This additional loss can be explained by increased turbulence intensity inside incoming boundary layer. Fig. 18 shows turbulence intensity profiles of incoming boundary layer. It tells higher turbulence intensity profiles as bigger size of roughness elements on endwall. It leads enhancing mixing by higher turbulence intensity within incoming boundary layer and this is thought to be the reason of additional loss. This is the different result from those of showing same inclined loss curve both incoming thin and thick boundary layer [12], [13], [14], [17].

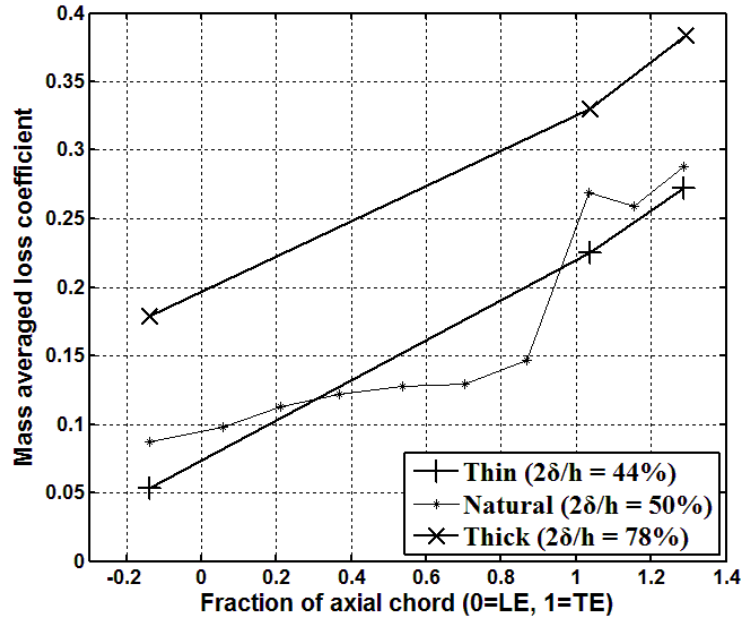

(a)

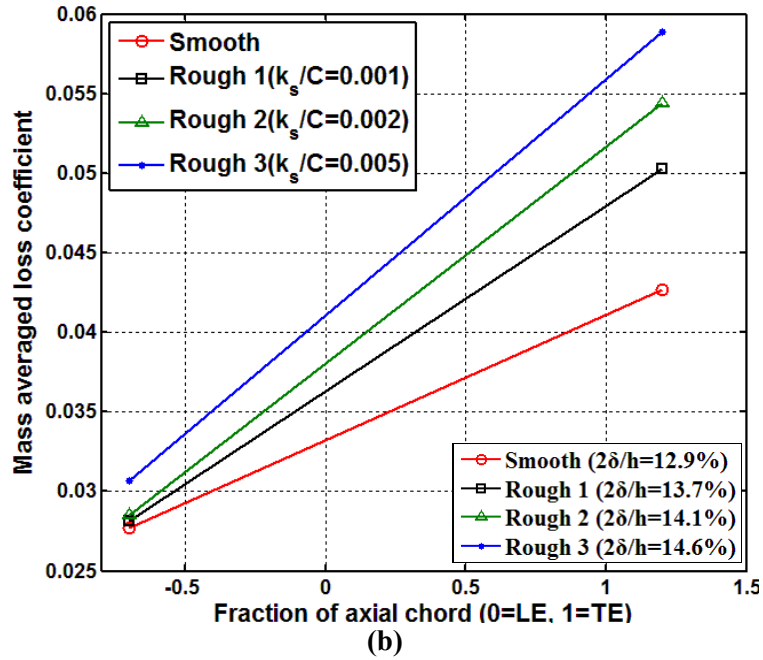

(b)

Fig. 17 Mass averaged loss coefficients between inlet and downstream of cascade; (a) Reproduced, thin and thick incoming boundary layer from Gregory-Smith and (b) Rough endwall cascade

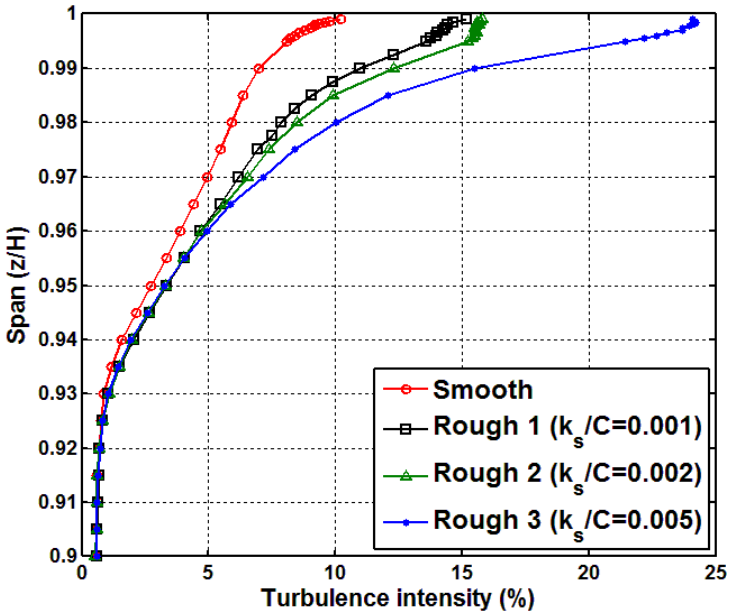

Fig. 18 Turbulence intensity profiles of incoming boundary layer

4. Conclusions

Mass averaged loss coefficients were increased from 0.043 to 0.050, 0.054, 0.059 from smooth to 0.001, 0.002 and 0.005 of k_s / C size of rough case respectively. Mass averaged loss coefficient was not linearly increased but saturated at rough 3 case (0.005 of k_s / C).

Above increments of mass averaged loss coefficients caused by higher secondary losses, especially stronger passage vortex was the main reason as bigger size of roughness adhered to the endwall. Saturation of mass averaged loss coefficients at rough 3 case was also explained saturated circulations which associated with passage vortex and counter vortex from smooth to rough 3 case due to adverse effects between the strengthen of incoming vortex and it's less stretching.

The bigger roughness on the endwall created the greater velocity deficit so that incoming normal voriticity within incoming endwall boundary layer was higher due to momentum loss by endwall surface roughness elements.

Above increment of incoming normal voriticity as attaching bigger size of roughness element to the endwall provoked stronger streamwise vorticities at the downstream of cascade which is following by classical secondary flow theories [8], [9].

Effect of variation of incoming boundary layer thickness was little by attaching roughness element to the endwall.

Additional loss was generated through blade passage by confirming comparing the loss difference between downstream and inlet for all rough cases.

The effects of casing roughness on aerodynamic performance, especially secondary loss in a linear turbine cascade have been addressed in this study. The new contributions of this study are as follows.

1. Experiments to investigate the effects of casing roughness in a turbine cascade are conducted by adhering sand grain on the linear cascade tip endwall.
2. Casing roughness makes overall loss increase.
3. But overall loss increment is not continuously rise but saturated as roughness size goes greater due to saturation of circulations of both region of passage vortex and counter vortex.
4. Saturation of circulations is due to adverse effects between strengthen of incoming vortex and it's less vortex stretching by reduced streamwise velocity due to higher momentum deficit from roughened endwall.
5. The major portion of overall loss increase is secondary loss, especially generated by passage vortex.

6. Casing roughness increases incoming normal vorticity by greater velocity deficit within incoming boundary layer, which causes strong streamwise vorticity at the downstream.
7. Additional loss happens due to greater turbulent mixing by higher turbulence intensity within the incoming boundary layer of rough cases, which is contrast to previous experiment results of thin and thick boundary layer.

References

[1] J.P. Bons, 2010, "A Review of Surface Roughness Effects in Gas Turbines,' ASME J. of Turbomachinery, vol. 132, pp. 021004-1-16.

[2] B. P. Casaday, A. A. Ameri, and J.P. Bons, 2013, "Numerical Investigation of Ash Deposition on Nozzle Guide Vane Endwalls," ASME J. of Engineering for Gas Turbines and Power, vol. 135, pp. 032001-1–9.

[3] Denton, J. D., 1993, "The 1993 IGTI Scholar Lecture: Loss Mechanisms in Turbomachines," ASME J. of Turbomachinery, vol. 115, No. 4, pp. 621-656.

[4] Sjolander, S. A., 1997, "Overview of Tip- Clearance effects in Axial Turbines," VKI Lecture Series 1997-01: Secondary and Tip Clearance Flows in Axial Turbines, Von Karman Institute for Fluid Dynamics.

[5] J.P. Bons, R. P. Taylor, S. T. McClain and R. B. Rivir, 2001, "The Many Faces of Turbine Surface Roughness," ASME J. of Turbomachinery, vol. 123, pp. 739-748.

[6] N. M. Rao, B. Gumusel, L. Kavurmacioglu and C. Camci, 2006, "Influence of Casing Roughness on the Aerodynamic Structure of Tip Vortices in an Axial Flow Turbine," ASME Turbo Expo 2006, GT2006-91011.

[7] H. Matsuda, F. Otomo, H. Kawagishi, A. Inomata, Y. Niizeki and T. Sasaki, 2006, “Influence of Surface Roughness on Turbine Nozzle Profile Loss and Secondary Loss,” ASME Turbo Expo 2006, GT2006-90828.

[8] Squire, H. B., and Winter, K. G., 1951, “The Secondary Flow in a Cascade of Airfoils in a Non-uniform Stream,” J. of Aeronautical Sciences, 18, pp. 271-277.

[9] W. R. Hawthorne, 1951, “Secondary Circulation in Fluid Flow,” Proceedings of the Royal Society London A, 206, pp.374-387

[10] W. R. Hawthorne, 1955, “Rotational Flow Through Cascades, Part 1: The components of vorticity,” Quart. J. Mech. And Applied Math., vol. VIII, Part 3, pp. 266-279

[11] D. R. Glynn, 1982, “Calculation of secondary flow in cascades including effects of Bernoulli surface distortion,” Int. J. Heat & Fluid flow, vol. 3, no.2, pp. 73-80

[12] L. S. Langston, M. L. Nice and R. M. Hooper, 1977, “Three-Dimensional Flow Within a Turbine Cascade Passage,” ASME J. of Engineering for Power, vol.99, pp.21-28.

[13] P. Marchal, and C. H. Sieverding, 1977, “Secondary Flows Within Turbomachinery Bladings,” AGARD CP. 214, Paper no. 11.

[14] D. G. Gregory-Smith, and C. P. Graves, 1983, “Secondary Flows and Losses in a Turbine Cascade,” in: Viscous Effects in Turbomachines, AGARD CP. 351, Paper no. 17.

[15] C. H. Sieverding, 1985, “Recent Progress in the Understanding of Basic Aspects of Secondary Flows in Turbine Blade Passages,” ASME J. of Engineering for Gas Turbines and Power, vol. 107, pp.248-257.

[16] Langston, L. S., 2001.“Secondary flows in Axial Turbines – A Review.” Annals of the New York Academy of Science, vol. 934, pp.11-26.

[17] H.P.Hodson and R.G.Dominy, 1987, “The off-Design performance of a low pressure turbine cascade,” ASME J. of Turbomachinery, vol.109, pp.201-209.

[18] I. H. Hunter, 1982, “Endwall Boundary Layer Flows and Losses in an Axial Turbine Stage,” ASME J. of Engineering for Power, vol. 104, pp.184-193.

[19] Sharma, O. P., and Butler, T. L., 1987.“Predictions of Endwall Losses and Secondary Flows in Axial Flow Turbine Cascades.” J. Turbomachinery, vol. 109, pp. 229-2336.

[20] Dring, R. P., Jolyn, H. D., and Blair, M. F., 1987, “The Effects of Inlet Turbulence and Rotor/Stator Interactions on the Aerodynamics and Heat Transfer of a Large-Scale Rotating Turbine Model,” NASA Contractor Report 179469 UTRC-R-86-956480-4.

[21] H. W. Coleman and W. G. Steele, 2009, “Experimentation, Validation, and Uncertainty Analysis for Engineers,” 3rd edition, John Wiley & Sons, Inc.

[22] Judd, A. M., “Calibration of a Five Tube Probe for Measuring Wind Speed and Direction,” Journal of Physics E; Scientific Instruments Vol. 8, 1975

[23] Everett, K. N., Gerner, A. A. and Durston, D. A., “Seven-Hole Cone Probes for High Angle Flow Measurement Theory and Calibration,” Journal of AIAA, 1983

[24] Kim, J. K. and Kang, S. H., “Full Angle Range Pressure Coefficient Maps of Five-Hole Probe and New Calibration Coefficients,” Journal of KSME, Vol. 21, 1997

[25] Matsunuma, T., Abe, H., and Tsutsui, Y., 1999, “Influence of Turbulence Intensity on Annular Turbine Stator Aerodynamics at Low Reynolds Numbers,” ASME Paper No. 99-GT-151

[26] C. C. Koch and L. H. Smith, 1976, “Loss Sources and Magnitudes in Axial-Flow Compressors,” Journal of Engineering for Power, vol. 98, pp. 411-424.

[27] J. P. Bons, 2014, personal communication.

[28] K. Bammert and H. Sandstede, 1972, “Measurements Concerning the Influence of Surface Roughness and Profile Changes on the Performance of Gas Turbines,” ASME Journal of Engineering for Power, vol. 122, pp. 207-213.

[29] H. Schlichting, 1960, “Boundary Layer Theory,” 4th edition, McGraw Hill, N.Y.

[30] D. G. Gregory-Smith, C. P. Graves, J. A. Walsh, “Growth of Secondary Losses and Vorticity in an Axial Turbine Cascade,” ASME J. of Turbomachinery, vol. 110, No. 1, pp. 1~8.

[31] M. Yaras, S. A. Sjolander, “Development of the Tip-Leakage Flow Downstream of a Planar Cascade of Turbine Blades: Vorticity Filed,” ASME J. of Turbomachinery, vol. 112, No. 4, pp. 609~617.

[32] Takayuki Matsunuma, 2005, “Effects of Reynolds Number and Freestream Turbulence on Turbine Tip Clearance Flow,” ASME J. of Turbomachinery, vol. 128, no.1, pp. 166-177.

[33] Michael J. Brear, H.P. Hodson, Paloama Gonzalez, Neil W. Harvey, 2002, “Pressure Surface Separations in Low-Pressure Turbines — Part 2: Interactions With the Secondary Flow,” ASME J. of Turbomachinery, vol. 124, no.3, pp. 402-409.

[34] G. D. Maclsaac, S. A. Sjolander, T. J. Praisner, 2012, “Measurements of Losses and Reynolds Stresses in the Secondary Flow Downstream of a Low-Speed Linear Turbine Cascade,” ASME J. of Turbomachinery, vol. 134, pp. 061015-1-12.

[35] R. A. Graziani, M. F. Blair, J. R. Taylor and R. E. Mayle, 1980, “An Experimental Study of Endwall and Airfoil Surface Heat Transfer in a Large Scale Turbine Blade Cascade,” ASME J. of Engineering for Power, vol. 102, pp. 257-267.

요약(국문초록)

터빈 캐스케이드에서 케이싱의 표면 거칠기가 공력 성능에 미치는 영향

케이싱의 표면 거칠기가 터빈 캐스케이드의 공력성능에 미치는 영향을 연구하기 위해 끝벽의 블레이드 상류에 3 가지 다른 크기(k_s=105, 180, 500μm)의 모래 알갱이로 표면 거칠기를 구현하여 블레이드 하류에서 전압 손실을 5 홀 프르브를 이용하여 측정하였다. 통로와류에 해당하는 2 차 손실의 증가가 전체적인 질량 평균 손실계수 증가의 원인임을 손실 계수 컨투어, 순환, 유동방향 소용돌이도 컨투어를 통해 확인했다. 끝벽의 표면 거칠기가 입구 유동의 경계층 특성을 변화시켜, 이에 따라 입구 유동의 소용돌이도가 커진 것이 블레이드 하류에서 통로 와류에 의한 손실을 증가시키는 원인이었다. 또한 끝벽의 표면 거칠기는 경계층 내의 난류 강도를 증가시켜 추가적인 2 차 손실을 발생시켰다.

주요어 :케이싱 표면 거칠기, 터빈 케스케이드, 통로 와류, 손실계수

학 번 : 2012-23174